Frontiers in Mechanochemistry and Mechanical Alloying

INCOME2008
1-4 December, 2008

ON THE PROCESSING OF DENSE HETERO-NANOSTRUCTURED METALLIC MATERIALS FOR IMPROVED STRENGTH / DUCTILITY BALANCE BY ECAE AND SPS METHODS

T. Grosdidier[1,ξ], G. Ji [1, 2], N. Llorca[3]
[1] Laboratoire d'Etude des Textures et Application aux Matériaux (LETAM), UMR CNRS 7078,
Université Paul Verlaine - Metz, Ile du Saulcy, 57045 Metz Cedex 01, France
[2]Presently with : Laboratoire de Métallurgie Physique et Génie des Matériaux (LMPGM), UMR CNRS 8517,
Université des Sciences et Technologies de Lille, Cité Scientifique, 59650 Villeneuve d'Ascq, France
[3]Department of Materails Science and Metallurgical Engineering, Facultat de Química,
University of Barcelona, C/Martí Franqués 1-11, 08028 Barcelona, Spain

Keywords: Electric current assisted sintering (ECAS), Spark plasma sintering (SPS), Mechanical milling (MA), Equal channel angular extrusion/pressing (ECAE/ECAP), Nanostructured metals (Hetero-nanostructure)

Abstract

This paper has examined some recent findings concerning the processing of fully dense hetero-nanostructured materials (i.e. consisting of nano, ultrafine and micrometric grains) which can be produced by using the interplay between heavy deformation and recrystallization. By plastic deformation of bulk materials, an improved strength/ductility balance can be obtained directly by imparting high strain deformation (by ECAE) until the occurrence of recrystallization. Using a powder metallurgy route, the strong potential of electric field assisted sintering (ECAS) techniques for producing multi-scale microstructures when a milled powder is used is demonstrated. In this case, in addition to modifying the classic processing parameters (time/temperature of SPS), altering the nature of the milled powder - by Y_2O_3 addition during the milling stage - is also a good way to delay the onset of recrystallization and, thereby, increase the fraction of ultrafine grains.

Introduction and Background to Present Research

Nanostructured bulk materials can be produced by a number of processing methods, which essentially fall into two categories: (i) severe plastic deformation of bulk microstructured materials and (ii) consolidation of nanoparticles or ultrafine-grained powders. In addition to these two broad categories, pulsed electro-deposition is also a well established technique to reduce grain size - down to about a few nm – that is however restricted to thick (20 microns or so) deposits. It has been found experimentally that the nanostructured metals produced by these techniques show a very high strength – typically several times higher than observed in coarse-grained materials - but a limited ductility of only a few percent of uniform elongation. For practical applications of nanostructured metals, it is therefore required to optimize the balance between strength and ductility. In a recent paper [1], Wang and Ma have explored - for intrinsically ductile metals - different ideas to remove or delay the plastic instabilities that hamper the useful ductility due to the presence of the nanostructure. The suggested stabilizing mechanisms were invoked by selecting appropriate tensile deformation conditions (such as deformation temperature and strain rate) or by tailoring the grain size structure in order to get bimodal or multi-modal grain size distributions [1]. For the latter case, even if the number fraction of larger grains in the nanostructure is low, their volume fraction can be sufficiently high to contribute to dislocation-based plasticity in the material [1]. Therefore, both thermomechanical and powder metallurgy approaches have been tested over the last years to produce this type of hybrid microstructures. For example, through thermo-mechanical treatments, Wang et al. produced Cu with a bimodal grain size (190 nm and 1700 nm) which exhibited a 65% total elongation to failure and retained a relative high strength [2]. Zhang et al. [3] have compacted cryomilled Zn powder at room temperature and varied the microstructure of nano-/ultrafine grain size by changing the milling times. Also, Shanmugasundaram et al. blended gas atomized and milled powders to obtained hot pressed samples having reasonable ductility and toughness [4]. Han et al. [5] produced bulk nanostructured Al alloys by hot/cold isostatic pressing followed by secondary extrusion of cryomilled powders. They pointed out that the nanostructured hybrid materials could be obtained by intentionally combining cryomilled (i.e. nanostructured), unmilled, and/or partially milled powders. All these processing routes lead to an optimized combination of high strength with fairly good ductility; confirming thereby that the microstructure usually contained a distribution of grain sizes for most of the nanocrystalline metals showing some ductility. In many of the tested processes, the intrinsic heterogeneity of the recrystallisation process is used to introduce some large recrystallized grains within a heavily deformed structure. Even if the combination of deformation and thermal cycles appears fairly easy to implement, the difficulty with such processing route lies in the exact control of the thermo-mechanical sequence to generate the suitable mixture in a fairly reproducible manner. Thus, alternative methods for processing materials with bimodal or broad grain size distributions such as electric current assisted sintering (ECAS) of milled powders [6] or direct current electro-deposition [7] have been recently proposed. The aim of the present contribution is to illustrate some alternative ways of producing multi-modal sub-micrometer grain sized materials using techniques involving either (i) severe plastic deformation of bulk microstructured materials and (ii) consolidation of ultrafine-grained powders.

ξ email: Thierry.grosdidier@univ-metz.fr

High Strain Deformation to Induce Recrystallization

Among the most advanced high strain deformation techniques are the high pressure torsion (HPT) [8,9], equal channel angular extrusion /pressing (ECAE/ECAP) [10,11], and accumulative roll-bonding (ARB) [12,13]. Due to structural and textural heterogeneities developed with these processes as well as a high content of stored energy, annealing of nanostructured metals is difficult to control because of the occurrence of non-uniform coarsening and recrystallization. These deformation heterogeneities are for example particularly present at the scale of the billet of ECAE processed materials [14-16]. Therefore, as also exemplified recently by the sub-surface heterogeneous recrystallized structures observed after one step annealing of ARD deformed samples [17], a two-step annealing procedure is often required to avoid discontinuous recrystallization [17]. Another effective route to create grain size heterogeneities, as illustrated in Fig.1, is to use recrystallization induced during the high straining process. Figure 1 illustrates, by longitudinal EBSD analysis, the microstructure evolution of a commercial purity Cu alloy processed by ECAE. The material was processed using the so-called route Bc, as detailed in [18], but for number of passes as high as 16. The development of texture and microstructure in Cu has been the subject of several publications including for example references [19,20]. As already demonstrated in many metals produced by ECAE, the grain size reduction can be roughly described by the "fragmentation" of the initial grains and the creation of sub-grains having an increased amount of misorientation with increasing strain; thus leading to ultra fine grains separated by high misorientation boundaries (Fig. 1(a) to 1(c)). In the case of this Cu, the samples processed for 12 passes and more retained a very heterogeneous structure consisting of a mixture of patches having different microstructures. They were broadly made of 3 types of grains: ultra fine equiaxed (similar to those in Fig. 1(c)), coarse and fairly equiaxe (some are visible in Fig. 1(d)) and medium elongated (similar to those in Fig. 1(b)). A detailed characterization of this microstructure and its formation mechanisms will be published elsewhere [21]. In short, it is formed as a result of a complex combination of dynamic and fairly static recrystallisation occurring at different stages of the ECAE process. Interestingly however, the microstructure was fairly similar after 12 or 16 passes. This indicates that pressing rods for many passes – at a controlled temperature depending on the deformed metal – can induce a balance between recovery/recrystallization and deformation processes to produce a multi-modal grain size distribution including a significant fraction of ultra fine grains.

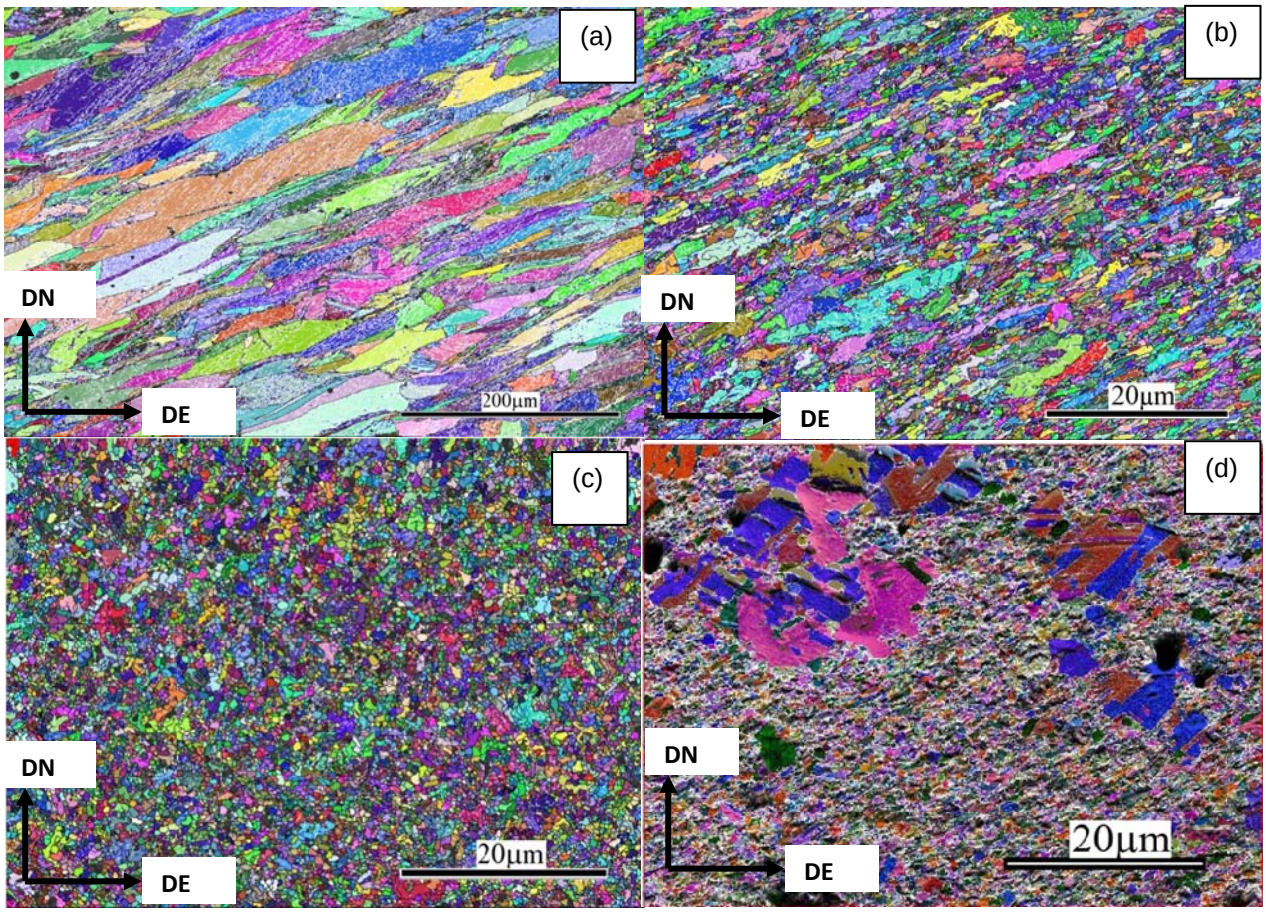

Figure 1. Evolution of the microstructure with increasing number of passes (route Bc) of ECAE-Cu: (a) 1 pass, (b) 2 passes, (c) 8 passes and (d) 12 passes

Figure 2 shows some tensile engineering stress-strain curves recorded on the ECAE-Cu samples deformed at different number of passes. It is clear from Fig 2(a) that the strength of the material increases gradually with the number of passes from 1 to 8. However, these curves peak soon after yielding, in sharp contrast to the behavior of the initial coarse grain material. Such very limited strain hardening is common to severely plastically deformed Cu due to the low capacity of dislocation storage [1, 22]. Comparatively, as more clearly visible in the enlarged image of Fig. 2(b), the strain hardening capability could be improved for the case of the heterogeneous microstructure obtained for the higher number of passes (12 and 16); leading to an improved strength/ductility balance. It is also interesting to notice in Fig. 2(a) that, despite different numbers of passes, the highly strained samples (12 and 16 passes) presented very similar mechanical response.

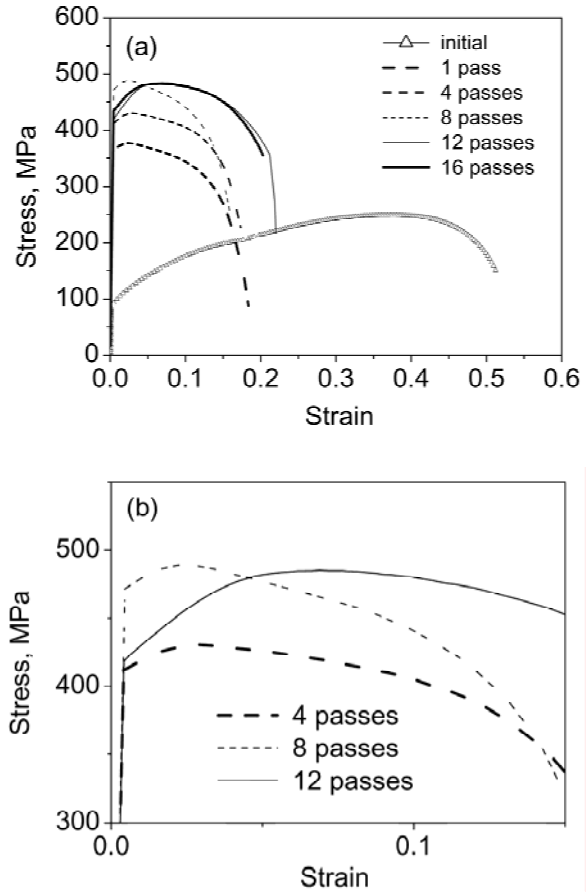

Figure 2. Tensile engineering stress/strain curves of the Cu samples processed for different passes of ECAE (route Bc)

Electric Current Assisted Sintering (ECAS) of Mechanically Milled Powders

A number of consolidation processes have been applied to fabricate nanostructured materials from milled powders such as cold pressing and hot extrusion [23-25], hot isostatic pressing and forging [25, 26], thermal/plasma spraying of thick deposits [27-31], and, more recently, techniques for which an electric current was used to aid the pressure assisted sintering [32-37]. A very complete and extended review has recently been published on these electric current activated/assisted sintering (ECAS) techniques that outlined their technological and economical advantages [38]. Different names and acronyms have been used to describe these processes which often involved the application of similar types of current waveform or the utilization of the same apparatus while, on the other hand, identical names have also been used to designate different processes. For example, the ECAS techniques cover various designations such as Spark Plasma Sintering (SPS), Pulsed Electric Current Sintering (PECS), Pulsed Discharge Sintering (PDS), Resistance Sintering (RS), etc [38]. In general, compared to other conventional methods, the use of the electric current during sintering authorises faster heating rates, lower sintering temperatures, much shorter holding times and the elimination of added processing agent. One of the advantages of this thermo-efficiency is the possibility to sinter nanostructured powders to near theoretical density with little grain growth or retention of metastability.

Multi-modal Grain Size Distribution by SPS of Milled Powder

TEM analysis have recently established that SPS samples processed from milled powders always contained grains having a broad range of grain sizes varying from tens of nm towards the micrometre range [35, 39, 40]. This is illustrated by the TEM bright field images given in Fig. 3 that were obtained from the same thin foil a consolidated sample obtained from a (0.2 % Y_2O_3 + FeAl) milled powder.

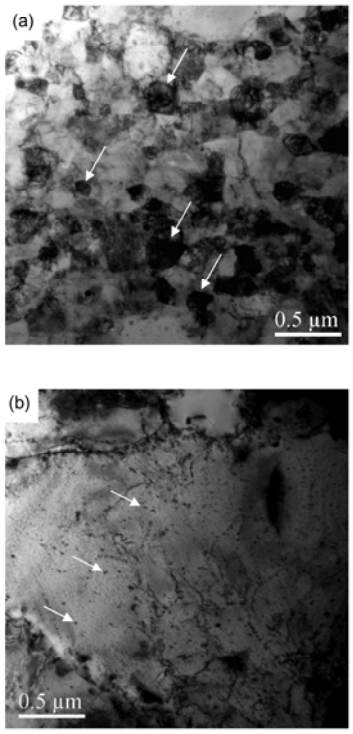

Figure 3. TEM bright-field micrographs illustrating the wide distribution of grains in ECAS/SPS sample sintered from a milled (FeAl + 0.2 %Y_2O_3) powder: nanometric grains (a) and a micrometric grain containing a fine distribution of oxides (b)

A detailed analysis of the microstructure of this type of Y_2O_3 reinforced FeAl sintered samples indicated that local thermal gradient as high as 600°C could be created during the ECAS sintering process [6,40]. These gradients, revealed at the scale of the powder, were witnessed by a detailed EDX and imaging analysis in the TEM [40] and the redistribution of Yttrium [40, 41]. The large grain size distribution was in fact controlled by combination of (i) these locally large temperature difference generated during the SPS process itself and (ii) the use of milled powder. Indeed, while fine grains are retained in the area where local temperature is relatively low, the Joule effect concentrates at the neck joining powder particles so that these areas are more rapidly heated and deformed plastically under the applied external pressure. Recrystallization and grain growth occurred more rapidly in the overheated areas where larger grains could form.

The EBSD maps in Fig. 4 show two examples of typical microstructures obtained by SPS of milled powder at, comparatively, low and high sintering temperatures [35, 40]. As seen by the black patches visible in Fig. 4(b), some porosity was still present for the low temperature regime. SEM also revealed that a thin oxide layer was formed at the surface of the powder particles [40]. Comparatively, increasing the sintering temperature causes the breakage of this thin oxide layer and a good densification can be obtained (as seen in Fig. 4(a)). The image in Fig. 4(b) also clearly reveals the presence of a badly milled powder particle for which 5 or 6 adjacent large grains are visible. In both cases however, the EBSD maps confirm that the variation in grain size of the materials obtained from the milled powder is quite considerable. The recent analysis of pure aluminium sintered by SPS from mechanically milled powders, performed by Kubota and Wynne [42], has also revealed a multi-modal grain size distribution. As could be expected from a powder metallurgy route, Kubota and Wynne have also shown that the sintered material was fairly isotropic (i.e. presenting no preferential texture component). It should also be mentioned that, as recrystallization is involved during the electric assisted sintering of the milled powder, an advantage of this processing route - over severe plastic deformation of massive parts - is the fact that high angle grain boundaries are directly created.

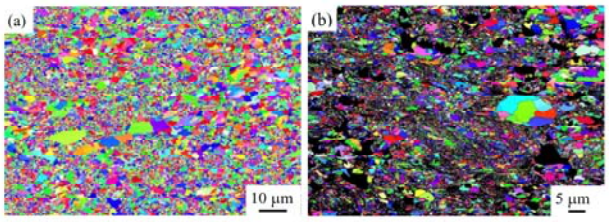

Figure 4: Typical EBSD maps of samples processed by electric current assisted sintering from milled FeAl powder at (a) 900°C (medium temperature range) and (b) 800°C (low temperature range)

Quantitative Analysis of Multi-scale Structures / Effect of the Starting Powder

EBSD maps were used to analyze quantitatively the microstructure of various materials sintered under different SPS processing conditions. The exact procedure for this has been detailed elsewhere [6,40]. In brief, the maps were recorded with a step size of 50 nm and grains containing two adjacent pixels or more having the same orientation were considered to be real grains. Figure 5(a) shows an example of OIM map obtained by EBSD analysis.

It is clear that the variation of grain size is quite considerable. In addition to nano-/ultrafine grains, some larger micrometric grains are also present. As for the EBSD map in Fig. 5(b), some extreme largest grains (arrowed - reaching about 6-7 µm) are also present and are due to the presence of a poorly milled powder particle. Examples of the treated OIM maps are shown in Figs. 5(b) to 5(e). In comparison with its original map shown in Fig. 5(a), the colored areas in Fig. 5(b) correspond to the unrecrystallized (i.e. still deformed) areas that were eventually retained in the end-product. These domains - that did not recrystallize or recover sufficiently - were witnessed by the fact that they emitted blurred Kikuchi patterns that could not be indexed; witnessing thereby the high amount of dislocations they still contained [6]. The treated maps of Figs. 5(c), 5(d) and 5(e) highlight the recrystallized grains for which the sizes are contained in the ranges 100-500, 500-1000 and above 1000 nm, respectively.

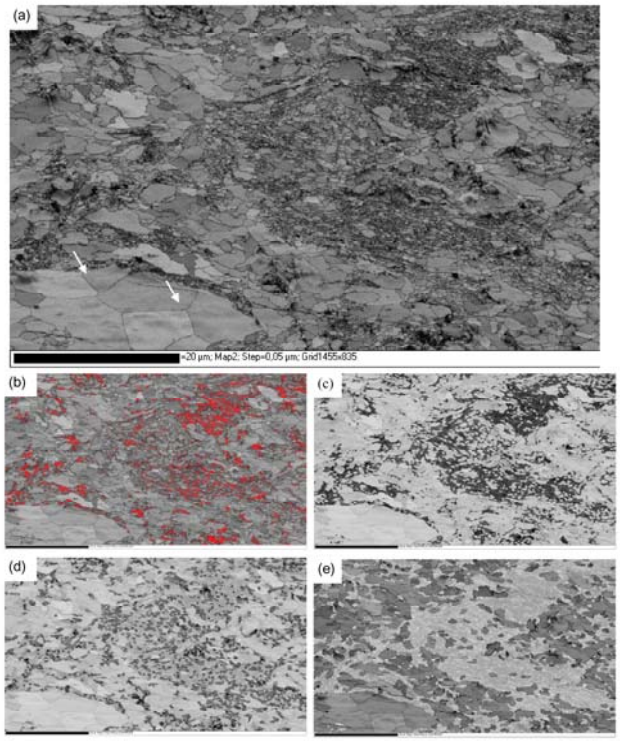

Figure 5. (a) Example of an as-obtained EBSD map (band contrast quality map) of an ECAS/SPS sintered sample; (b) corresponding treated OIM map showing the unrecrystallized areas (red contrast); (c), (d) and (e) corresponding treated OIM maps highlighting the grain area fractions (dark grey contrasts) in the size ranges 100-500, 500-1000 and above 1000 nm, respectively. Note the large grains associated with the presence of a poorly milled power particle (arrowed)

Using this procedure, the effect of the nature of the initial powders – atomized (microcrystalline), milled (nano-structured) with or without Y_2O_3 reinforcement – on the grain size

distribution has also been studied. Figure 6 gives a plot showing the number of grains contained within the +100/-500 nm, +500/-1000 nm and +1000 nm grain size fractions for the case of the processing of different types of FeAl powders. All the grains of the sample obtained from the atomised powder are above 1 μm with an average size close to 5.2 μm. In contrast, the sample obtained from milled powder (without Y_2O_3) contained a significant amount (about 50%) of grains having a size below 500 nm. With an average grain size of about 570 nm, only 15 % of the grains are in the highest size fraction with their average size centred on 1350 nm.

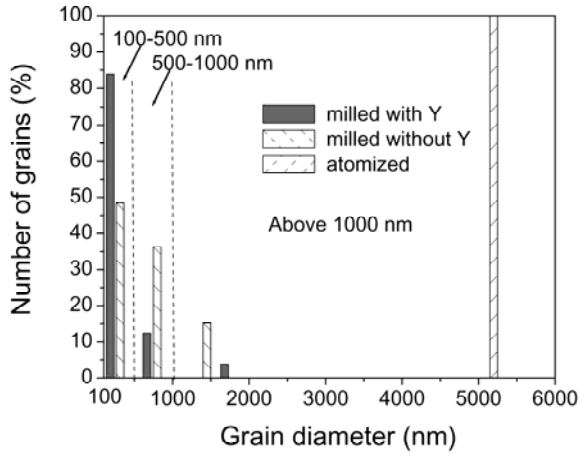

Figure 6. Graph showing the number of grains and their average size within the +100/-500 nm, +500/-1000 nm and +1000 nm grain size fractions for different types of initial powder (atomized FeAl powder, milled FeAl powder, milled FeAl powder with Y_2O_3 addition)

The effect of the Y_2O_3 introduction during the milling procedure is essentially to delay the recrystallization process. Indeed, the sample processed from the Y_2O_3 reinforced milled powder also consisted of intermixed ultrafine and microcrystalline zones but also contained about 10% of grains that were still in a fairly deformed state [6]. Consequently, the average grain size was only 330 nm [6]. Also, more than 80 % of the grains are in the size range +100/-500 nm (Fig. 6). They coexist with about 10 % of the grains in the size range +500/-1000 nm and less than 5% of micrometric grains.

Conclusion

In conclusion, this paper has examined recent findings concerning the processing of fully dense hetero-nanostructured parts (i.e. consisting of nano, ultrafine and micrometric grains). Such types of hybrid microstructures can be produced efficiently by using the interplay between heavy deformation and recrystallization processes. This can be done for example by imparting high strain deformation using ECAE until the occurrence of recrystallization. Also, the strong potential of electric field assisted sintering (ECAS) is demonstrated. The two necessary conditions for the formation of such a multi-modal nano-grain structure are (i) the large temperature differences that are spontaneously generated during the ECAS/SPS process and (ii) the use of the milled powder within which the heavily-deformed nanostructure is present. It is also shown that modification of the milled powder by Y_2O_3 addition during the milling stage is a good way to delay the onset of recrystallization and, thereby, increase further the fraction of ultrafine grains.

Acknowledgment

The authors would like to thank Dr. D. Goran, and Mr N. Lugo for their help with some of the experiments.

References

1. Y.M. Wang and E. Ma, *Acta Mater*., 52 (2004) 1699.
2. Y.M. Wang, M.W. Chen, F.H. Zhou and E. Ma, *Nature* 419 (2002) 912.
3. X. Zhang, H. Wang, R.O. Scattergood, J. Narayan, C.C. Koch, A.V. Sergueeva and A.K. Mukherjee: *Acta Mater*,. (2002), 4823.
4. T. Shanmugasundaram, V.S. Sarma, B.S. Murty, M. Heilmaeir, Mater. Sci. Forum, 584-586 (2008) 97-101.
5. B.Q. Han and E.J. Lavernia, *Adv. Eng. Mater.,* 7 (2005) 457.
6. T. Grosdidier, G. Ji , and S. Launois, *Scripta Mater*. (2007) 525.
7. X. Shen, J. Lian, Z. Jiang and Q. Jiang, *Mat. Sci. Eng. A*, 487 (2008) 410.
8. R.Z. Valiev, R.K. Islamgaliev and I.V. Alexandrov, *Prog Mater. Sci,*. 45 (2000) 103.
9. G. Sakai, Z. Horita and T.G. Langdon, *Mater. Sci. Eng. A*, 393 (2005), p. 344.
10. V.M. Segal, *Mater. Sci. Eng. A*, 197 (1995) 157.
11. R.Z. Valiev and T.G. Langdon, *Prog Mater. Sci.,* 51 (2006) 881.
12. Y. Saito, H. Utsunomiya, N. Tsuji and T. Sakai, *Acta Mater.*, 47 (1999) 579.
13. N. Tsuji, Y. Ito, Y. Saito and Y. Minamino: *Scripta Mater.*, 47 (2002) 893.
14. A. Tidu, F. Wagner, W.H. Huang, P.W. Kao, C.P. Chang and T. Grosdidier, *J. Phys. IV*, 10 (2000) 211.
15. S. Li, I.J. Beyerlein, C.T. Necker, D.J. Alexander and M. Bourke, *Acta Mater.*, 52 (2004) 4859.
16. T. Grosdidier, J.-J. Fundenberger, D. Goran, E. Bouzy, S. Suwas, W. Skrotzki and L.S. Toth, *Scripta Mater.*, 59 (2008) 1087.
17. N. Kamikawa, X. Huang and N. Hansen: *J. Mater. Sci.*, 43 (2008) 7313.
18. N. Lugo, N. Llorca, J.M. Cabrera and Z. Horita: *Mat. Sci. Eng. A,* 477 (2008) 366.
19. H.W. Huang, L. Chang, P.W. Kao and C.P. Chang: *Mater. Sci. Eng. A*, 307 (2001) 113.
20. F. Dalla Torre, Lapovok R., J. Sandlin, P.F. Thomson, *Acta Mater.* 52 (2004) 4819.
21. T. Grosdidier, D. Goran, N. Ludo and N. Llorca, in preparation.
22. Y.S. Li, Y. Zhang, N.R. Tao and K. Lu, *Scripta Mater.*, 59 (2008) 475.
23. D.G. Morris and M.A. Morris, *Acta Metal. Mater,*. 39 (1991) 1763.
24. K.I. Moon and K. S. Lee, *J. Alloys Comp.* 291 (1999) 312.
25. A.P. Newbery, B. Ahn, T.D. Topping, P.S. Pao, S.R. Nutt and E.J. Lavernia, *J. Mater. Proc. Technol.*, 203 (2008) 37.

26. S. Revol, S. Launois, R. Baccino, G. Le Marois and B. Rigal, *Fusion Eng. Design*, 58 (2001) 751.
27. T. Grosdidier, A. Tidu and H.L. Liao, *Scripta Mater.*, 44 (2001) 387.
28. J. He and J.M. Schoenung, *Mater. Sci. Eng. A*, 336 (2002) 274.
29. J. Gang, J.P. Morniroli and T. Grosdidier, *Scripta Mater.*, 48 (2003) 1599.
30. S.C. Tjong and H. Chen: *Mat. Sci. Eng.* R, 45 (2004) 1.
31. G. Ji, T. Grosdidier, H.L. Liao, J.P. Morniroli and C. Coddet, *Intermetallics*, 13 (2005) 596.
32. M. Omori *Mater. Sci. Eng., A*, 287 (2000) 183.
33. S.H. Lee, K.I. Moon, H.S. Hong and K.S. Lee, *Intermetallics*, 11 (2003) 1039.
34. Y. Minamino, Y. Koizumi, N. Tsuji, N. Hirohata, K. Mizuuchi and Y. Ohkanda, *Sci. Tech. Adv. Mater.*, 5 (2004) 133.
35. T. Grosdidier, G. Ji, F. Bernard, E. Gaffet, Z.A. Munir and S. Launois, *Intermetallics*, (2006) 1208.
36. G. Ji, D. Goran, F. Bernard, T. Grosdidier, E. Gaffet and Z. A. Munir, *J. Alloys Comp.*, 420 (2006) 158.
37. A. Zuniga, L. Ajdelsztajn and E.J. Lavernia, *Metall. Mater. Trans. A*, 37 (2006) 1343.
38. R. Orrù, R. Licheri, A.M. Locci, A. Cincotti and G. Cao, *Mater. Sci. Eng. R*, 63 (2009) 127.
39. G. Ji, T. Grosdidier, F. Bernard, S. Paris, E. Gaffet and S. Launois, *J. Alloys Comp.*, 434-435 (2007) 358.
40. G. Ji, T. Grosdidier, N. Bozzolo and S. Launois, *Intermetallics*, 15 (2007) 108.
41. T. Grosdidier, G. Ji and N. Bozzolo, *Intermetallics*, 14 (2006) 715.
42. M. Kubota and B.P. Wynne, *Scripta Mater.*, 57 (2007) 719.